SLAC–PUB–5101
UC–IIRPA-89-02
September 1989
(E)

A Measurement of the Total Hadronic Cross Section in Tagged $\gamma\gamma$ Reactions *

H. Aihara,[n] M. Alston-Garnjost,[i] R.E. Avery,[i] A.R. Barker,[h] D.A. Bauer,[h] A. Bay,[i]
R. Belcinski,[j] H.H. Bingham,[b] E.D. Bloom,[m] C.D. Buchanan,[e] D.O. Caldwell,[h]
H-Y. Chao,[a] S-B. Chun,[e] A.R. Clark,[i] G.D. Cowan,[i] D.A. Crane,[j] O.I. Dahl,[i] M. Daoudi,[f]
K.A. Derby,[i] J.J. Eastman,[i] P.H. Eberhard,[i] T.K. Edberg,[i] A.M. Eisner,[d] F.C. Erné,[l]
K.H. Fairfield,[m] A. Fridman,[e] G. Godfrey,[m] J.M. Hauptman,[a] C. Ho,[f] W. Hofmann,[k]
T. Kamae,[n] R.W. Kenney,[i] S. Khacheryan,[e] R.R. Kofler,[j] D.J. Lambert,[i]
W.G.J. Langeveld,[f] J.G. Layter,[f] W.T. Lin,[f] F.L. Linde,[l] S.C. Loken,[i] A. Lu,[h] G.R. Lynch,[i]
J.E. Lys,[b] R.J. Madaras,[i] B.D. Magnuson,[d] H. Marsiske,[m] G.E. Masek,[g] L.G. Mathis,[i]
S.J. Maxfield,[j] R.R. McNeil,[c] E.S. Miller,[g] N.A. Nicol,[i] D.R. Nygren,[i] P.J. Oddone,[i] H. Oh,[f]
Y-T. Oyang,[e] H.P. Paar,[g] A.P.T. Palounek,[i] S.K. Park,[a] D.E. Pellett,[c] M. Pripstein,[i] M.T. Ronan,[i]
R.R. Ross,[i] F.R. Rouse,[i] K.A. Schwitkis,[h] J.C. Sens,[l] G. Shapiro,[i] B.C. Shen,[f] J.R. Smith,[c]
J.S. Steinman,[e] R.W. Stephens,[h] M.L. Stevenson,[i] D.H. Stork,[e] M.G. Strauss,[j] M.K. Sullivan,[d]
T. Takahashi,[n] S. Toutounchi,[j] G.J. VanDalen,[f] R. van Tyen,[i] W. Vernon,[g] W. Wagner,[c]
E.M. Wang,[i] Y-X. Wang,[d] W.A. Wenzel,[i] Z.R. Wolf,[i]
H. Yamamoto,[e] S.J. Yellin,[h] G.P. Yost,[a] G. Zapalac,[m] and C. Zeitlin[c]

TPC/Two-Gamma Collaboration

[a] *Ames Laboratory, Iowa State University, Ames, Iowa 50011*
[b] *University of California, Berkeley, California 94720*
[c] *University of California, Davis, California 95616*
[d] *University of California Intercampus Institute for Research at Particle Accelerators, Stanford, California 94305*
[e] *University of California, Los Angeles, California 90024*
[f] *University of California, Riverside, California 92521*
[g] *University of California, San Diego, California 92093*
[h] *University of California, Santa Barbara, California 93106*
[i] *Lawrence Berkeley Laboratory, University of California, Berkeley, California 94720*
[j] *University of Massachusetts, Amherst, Massachusetts 01003*
[k] *Max Planck Institute für Kernphysik, Heidelberg, Germany*
[l] *National Institute for Nuclear and High Energy Physics, Amsterdam, The Netherlands*
[m] *Stanford Linear Accelerator Center, Stanford University, Stanford, California 94309*
[n] *University of Tokyo, Tokyo, Japan*

Submitted to *Physical Review D*

* Work supported in part by Department of Energy contracts DOE–W–7405–Eng–82, DE–AT03–89ER40492, DE–AS03–76ER70285, DE–AT03–88ER40384, DE–AT03–87ER40327, DE–AT03–79ER70023, DE–AC03–76SF00098, DE–AC02–85ER40194, and DE–AC03–76SF00515, the National Science Foundation (under grants PHY89–07526 and PHY88–19536), the Joint Japan-United States Collaboration in High Energy Physics, and the Foundation for Fundamental Research on Matter in The Netherlands.

ABSTRACT

We present a measurement of the total cross section for $\gamma\gamma \rightarrow$ hadrons, with one photon quasi-real and the other a spacelike photon of mass-squared $-Q^2$. Results are presented as a function of Q^2 and the $\gamma\gamma$ center-of-mass energy W, with the Q^2 range extending from $0.2\,\mathrm{GeV}^2$ to $60\,\mathrm{GeV}^2$, and W in the range from 2 to 10 GeV. The data were taken with the TPC/Two-Gamma facility at the SLAC e^+e^- storage ring PEP, which was operated at a beam energy of 14.5 GeV. The cross section exhibits a gentle fall-off with increasing W. Its Q^2-dependence is shown to be well-described by an incoherent sum of vector-meson and point-like scattering over most of the observed W range. Agreement at high Q^2 is improved if a minimum p_T cutoff (motivated by QCD) is imposed on the point-like contribution.

I. INTRODUCTION

Inclusive hadron production in photon-photon collisions has been the subject of considerable theoretical and experimental work in recent years, as is documented in a number of reviews.[1–5] Much of the experimental focus has been on measuring the structure function F_2^γ of a quasi-real "target" photon, using a highly-virtual (spacelike) photon as a probe. In this domain - with Q^2, the negative of the probe photon's invariant mass squared, significantly larger than $1\,\mathrm{GeV}^2$ - a major fraction of the events is expected to result from pointlike interactions of photons and quarks. Consequently, there has been interest in comparisons to QCD predictions. On the other hand, measurements extending to low Q^2 have generally been presented in terms of total cross sections for $\gamma\gamma \to$ hadrons, and compared to models emphasizing the hadron-like (and particularly vector-meson-like) behavior of real or low-Q^2 photons. This approach allows making contact with the $Q^2 \to 0$ limit, where the hadron-like behavior is most dominant. (There is of course no clear-cut boundary between the point-like and hadronic domains.) In this paper we report total cross section results from data collected with the TPC/Two-Gamma Facility at the SLAC e^+e^- storage ring PEP, operated at a beam energy of 14.5 GeV. These data were previously presented[6,7] in terms of F_2^γ; however, for reasons to be explained shortly, the cross section values cannot be inferred from the F_2^γ values.

In e^+e^- storage rings, the two-photon reaction proceeds via the emission of space-like photons by the incoming e^+ and e^-, as shown in Fig. 1. The $\gamma\gamma$ cross section depends only on the invariant mass of the $\gamma\gamma$ system, W, and the masses $-q_i^2 = Q_i^2 = 4EE_i' \sin^2(\theta_i/2)$ of the photons. Each photon can be tagged by detecting the corresponding $e^\pm$, and measurements can be classified according to

the number of such "tags". One can also restrict one or both photons to being quasi-real by "anti-tag" cuts; i.e., one requires that there is no evidence for a scattered $e^{\pm}$ above a minimum detection angle (26 mrad in our case). In a measurement in which one photon is tagged and the other anti-tagged, one can write[8] $\sigma_{ee\to eeX} = L_{TT}(\sigma_{TT} + \epsilon\sigma_{LT})$. The subscripts T and L refer to transversely- and longitudinally-polarized photons, respectively. The luminosity functions L_{ij} are given in $O(\alpha^4)$ QED in Ref. 8, and $\epsilon = L_{LT}/L_{TT} \approx 1$ for the present experiment. One thus measures an effective cross section, $\sigma_{\gamma\gamma}(W, \mathrm{Q}^2) \approx \sigma_{TT} + \sigma_{LT}$, for a virtual photon on a real photon.

In single-tag reactions, the total cross section and the photon structure function are related by $\sigma_{\gamma\gamma}(W, \mathrm{Q}^2) = 4\pi^2\alpha \mathrm{F}_2^{\gamma}(x, \mathrm{Q}^2)/\mathrm{Q}^2$, where $x \equiv \mathrm{Q}^2/(\mathrm{Q}^2 + W^2)$, and Q^2 refers to the tagged photon. Given these relationships, one might hope to convert measured structure functions directly to cross sections. This, however, is impractical, for two reasons. First, particularly for larger x (small W), if a two-dimensional bin in x and Q^2 is transformed to a bin in W and Q^2, it is no longer rectangular: its W limits vary strongly with Q^2 across the bin. Second, in practice, one measures x_{vis} or W_{vis}, which differ from true values due to the effects of particle losses and detector resolution. To extract measurements of distributions depending on the true values of x or W requires an unfolding procedure[9] which minimizes correlations between adjacent data points in the space of the variable being measured. Hence, to determine the cross section, one should unfold the data directly in W rather than convert from $\mathrm{F}_2^{\gamma}(x)$ results, which are unfolded in x.

We have recently published[6] a detailed account of a measurement of the structure function in the range $0.2 < \mathrm{Q}^2 < 6.8\,\mathrm{GeV}^2$. We have also presented[7] results

on F_2^γ at high Q^2, $10 < Q^2 < 60\,\mathrm{GeV}^2$. Here we report on a measurement of $\sigma_{\gamma\gamma}(W, Q^2)$ using the same data as in the structure function measurements, but unfolded in W rather than x. We discuss the interpretation of the cross section in terms of vector dominance models (VDM) and the quark parton model (QPM). We also make comparisons to previous cross section measurements, of which two[10,11] are single-tagged, one[12] uses double-tagging with both photons off-shell, one[13] uses 0°-double-tagging, and one[14] is untagged.

II. THEORETICAL CONSIDERATIONS

The single-tag cross section contains contributions from at least three sources: a) pure vector-meson scattering; b) photon vector-meson scattering; and c) the point-like interaction of a photon and a quark. In a), both photons convert to vector mesons and interact, in analogy to other hadron-hadron reactions. This process is expected to contribute mainly at low $Q^2 (< 1\ \mathrm{GeV}^2)$, and to fall as $1/Q^4$ at large Q^2 due to the vector-meson propagator associated with the off-shell (probe) photon. As the probe gets more off-shell, process b) sets in; here, the point-like probe scatters from the hadron-like target photon. Processes a) and b) each involve at least one vector-meson-dominated photon, and lead to final states with limited p_T with respect to the collision axis. In contribution c), for which we use the QPM, the quark p_T in the center-of-mass is limited only by phase space. There is theoretical controversy[15] regarding the low-p_T contribution from QPM: below some value, confinement effects are probably overwhelming, making this process indistinguishable from process b). Thus, an incoherent sum of QPM and the vector-meson-dominated processes may well double count. It has been

suggested[15] that a minimum p_T cutoff be applied to the outgoing quarks in the QPM to avoid this. In Section V, we use a model with such a cutoff.

III. APPARATUS, DATA SELECTION, AND BACKGROUNDS

For this measurement, charged particles at angles greater than 350 mrad with respect to the beam axis were detected in the Time Projection Chamber (TPC), which simultaneously measured momentum and ionization energy loss, dE/dx. The $0.4\,T$ magnetic field allowed a momentum resolution at large angles of $\delta p/p = \sqrt{(0.06)^2 + (0.035p)^2}$, p in GeV. Small-angle charged particles, in the range 28–180 mrad, were detected in 15 planes of drift chambers arranged in 5 layers. Cylindrical drift chambers at smaller and larger radii than the TPC were used for triggering. Muon detectors covered 98% of 4π in solid angle. Neutral particles at large angles were detected in a hexagonal Geiger-mode calorimeter (HEX), and at smaller angles in the proportional-mode Pole-tip calorimeters (PTC), lead-scintillator Shower Counter (SHW), and NaI. The latter three calorimeters were also used as tagging devices. For those events with PTC tags (the high-Q^2 data), only final state particles in the central detector were utilized; for events with tags in the NaI or SHW (the low-Q^2 data), final state particles in the forward detector were used as well. Further details of the TPC/Two-Gamma Facility can be found in the literature.[16] The low-Q^2 data come from an integrated luminosity of 49 pb^{-1}, and were triggered by a tag in the NaI or SHW in coincidence with evidence of a track in the central detector. The high-Q^2 data come from 70 pb^{-1} of data taken with triggers that depended only on the central detector.

The details of the low-Q^2 structure function analysis have been published in Ref. 6. The data selection for the high-Q^2 analysis[7] is similar. Briefly stated, a high-energy tag was required in addition to at least three other particles, at least two of which had to be charged. A tag was defined by an energy cluster of at least 8 GeV in the NaI or SHW calorimeters, or at least 6 GeV in the PTC. In order to reduce the background from annihilation processes, particularly radiative annihilation, a charged track was required to point to this energy deposition. To provide anti-tagging, events were rejected if there was a calorimeter deposition with an energy greater than 4 (3) GeV opposite the tag in the low- (high-) Q^2 analysis. Of the charged particles other than the tag, at least one had to be identified as an unambiguous hadron or a π/μ ambiguity by the TPC dE/dx and momentum measurements. If there were only two charged particles other than the tag, and both were compatible with muons, the event was rejected if either one had associated hits in the muon chambers; this cut reduced contamination from radiative μ pair production. The invariant mass of the observed final state, W_{vis}, was required to be at least 1.0 GeV for the low-Q^2 data and 1.5 GeV for high-Q^2. Additional cuts were made to reduce the background from multi-hadron annihilation events: in the low- (high-)Q^2 data, the total visible energy (including the tag) was required to be less than 23 (20) GeV; in the high-Q^2 data only, the net longitudinal momentum was required to have an absolute value greater than 4 GeV. The total transverse momentum of all observed particles including the tag was required to be less than 2 (3) GeV for the low- (high-) Q^2 data.

Beam-gas backgrounds totalling roughly 10% in the low-Q^2 data and 1.5% in the high-Q^2 data were subtracted using the sidebands of the vertex z distribu-

tions. Three other classes of backgrounds were estimated by Monte Carlo calculations and, when non-negligible, subtracted bin-by-bin from the data. These classes are: (*i*) $\gamma\gamma$ production of lepton pairs; (*ii*) the inelastic-Compton contribution to $e^+e^- \rightarrow e^+e^-$ + hadrons; and (*iii*) e^+e^- annihilation. We found $\gamma\gamma \rightarrow \tau^+\tau^-$ contamination to be less than 2% in the low-Q^2 data and 5.6% in the high-Q^2 data. Background from $\gamma\gamma \rightarrow e^+e^-, \mu^+\mu^-$ was negligible in both samples. The inelastic-Compton cross section was negligible at low Q^2, but at high Q^2 was estimated to be 4.5%. The annihilation background was also negligible at low Q^2 due to the small number of hadrons (which might fake a tag) going into the tagging devices compared to the large number of genuine tags. At higher Q^2, the number of tags decreased relative to the number of hadrons, necessitating a Monte Carlo subtraction amounting to 6.4%.

IV. MONTE CARLO SIMULATION AND UNFOLDING

For both the low- and high-Q^2 analyses, Monte Carlo events were generated to determine the effects of detector efficiency and resolution. These events were used by a program[9] which then unfolded the data from W_{vis} to W. (A brief summary of the procedure is provided in the Appendix to this paper.) Two models were used: Model A produced $q\bar{q}$ pairs with limited p_T with respect to the collision axis, in the spirit of the VDM processes discussed above, while in Model B the angular distribution of the $q\bar{q}$ was the same as for the muons in $\gamma\gamma \rightarrow \mu^+\mu^-$. Fragmentation of the partons was carried out according to the Lund string model.[17] Proper modeling of the hadronic final state is essential since the unfolded cross section

is highly dependent on both the event detection efficiency and the detailed correlation of W_{vis} with W, as determined from the Monte Carlo detector simulation. We found earlier[6] that after iteratively adjusting the fragmentation parameters and the mixture of Models A and B, the topological features (multiplicity, neutral fraction, sphericity, etc.) of the Monte Carlo events (weighted by the unfolded structure function) agreed well with those of the data; we take this as evidence for the adequacy of our model. The unfolded structure function was found to be sensitive only at the 10% level to substantial changes in the fragmentation parameters and mixture. The high-Q^2 results are even less sensitive to the admixture of Models A and B, since the transverse boost from the tag is so great.

A detailed presentation of the systematic errors in the low-Q^2 measurement was given in Table 3 of Ref. 6. For $1.5 < W < 3$ GeV, the dominant error for that measurement comes from uncertainty in the fragmentation model. Added in quadrature with the other uncertainties (detector simulation, luminosity, trigger efficiency, backgrounds, radiative corrections, and target mass effects) we arrived at a 13–14% systematic error, depending slightly on Q^2. For $W > 3$ GeV, the uncertainty in the fragmentation model is reduced, and the total systematic error is 10–11%. The high-Q^2 data have a similar systematic error of approximately 15%. As some of the systematic uncertainties in our high- and low-Q^2 measurements are correlated, we assume no relative systematic errors between the two data sets when we combine them.

V. RESULTS

A. W Dependence of σ in Q^2 Bins

The results of the W unfolding of our data can be presented in several different ways. Owing to limited statistics at high Q^2, we used only the low-Q^2 data for obtaining cross sections in small bins of W. Fig. 2a and 2b show our unfolded cross section as a function of W in Q^2 bins (0.2–0.65 GeV^2 and 3.75–6.8 GeV^2, respectively) chosen to facilitate comparison with results from the PLUTO collaboration,[10] which are also shown. Since each experiment's systematic errors are highly correlated from bin to bin, we have chosen to display the results with the statistical errors only. (PLUTO's systematic uncertainties average 15% for W between 2 and 8 GeV, and are about 25% for $W < 2\,GeV$ and $W > 8\,GeV$.) At an average Q^2 of $0.44\,GeV^2$ (Fig. 2a), a large systematic discrepancy between our results and PLUTO's is evident for $W > 3\,GeV$. At the higher Q^2 illustrated in Fig. 2b, our data are slightly lower than PLUTO's, despite our lower average Q^2 ($4.4\,GeV^2$ vs. $5.4\,GeV^2$). Taken together, the implication of these comparisons at low and high Q^2 is a substantial difference in the measured Q^2 dependences of the cross section. This point is also discussed in Section V.C, in the context of fits to the Q^2 dependence.

B. Extrapolation to $Q^2 = 0$

As will be discussed, most of our low-Q^2 data are reasonably fit by a Generalized Vector Dominance Model[18] (GVDM) form factor. This form factor was used by PLUTO[11] to extrapolate their single-tag data with $0.1 < Q^2 < 1.0\,GeV^2$ to

$Q^2 = 0$, and by the Two-Gamma collaboration[12] to extrapolate their double-tag data with $Q^2 < 1.6\,\mathrm{GeV}^2$. We also used this form factor to extrapolate our data with $0.2 < Q^2 < 1.6\,\mathrm{GeV}^2$ to $Q^2 = 0$ by reweighting events in the unfolding step. The resulting cross section[19] is shown in Fig. 3. The extrapolation introduced additional systematic uncertainty in two ways. First, by varying the details of the unfolding (see the Appendix) and by comparing to direct fits of the results unfolded in narrow Q^2 bins, we estimated an uncertainty of 10%. This implies overall systematic uncertainties for the extrapolated results of 17% for $W < 3\,\mathrm{GeV}$ and 14% for $W > 3\,\mathrm{GeV}$. Second, the effect of varying the form of the extrapolating function among choices that give comparable fit quality could contribute up to 15% additional uncertainty. However, in order to facilitate comparisons with the earlier experiments, which do not allow for such an error, we have not added it into our total uncertainty.

The PLUTO and Two-Gamma results are also shown in Fig. 3. The present result agrees well with the Two-Gamma result for $4 < W < 10$, and the two are in reasonable agreement at lower W when systematic errors are taken into account. (The Two-Gamma systematic errors were 17% for W between 5 and 11 GeV, and 23% elsewhere.) Although the Two-Gamma measurement used the same apparatus as the present analysis, W was measured by the double-tag missing mass, so that no unfolding from W_{vis} to W was required. Also, the backgrounds and sources of systematic uncertainty were mostly distinct. Thus, the two measurements are largely independent. On a point-by-point basis, the PLUTO results are compatible with both the Two-Gamma and the present results, given systematic uncertainties. However, each experiment's systematic uncertainties are likely to

be highly correlated between W bins, so they cannot account for the differences in shape. Hence our measurement and the Two-Gamma measurement show a significantly milder rise in the cross section at low W than does PLUTO's. (Fits to the form $\sigma = A + B/W$ support this conclusion, but the values of A and B are highly sensitive to unfolding details and correlations. Such fits are discussed in the Appendix.) The most recent preliminary results from PLUTO's analysis[14] of the untagged total cross section and from the MD-1 experiment[13,5] both show little or no increase at low W.

C. Q^2 Dependence of the Cross Section

Figure 4 shows the Q^2 dependence of the cross section in four bins of W. We began by fitting the low-Q^2 data in rather narrow bins of W to four hypotheses: a) VDM, as defined below; b) GVDM[18]; c) VDM + QPM; and d) GVDM + QPM. For each case, we parameterized the non-QPM part of the cross section by $\sigma_{hadronic}(W, Q^2) = \sigma_0(W)F(Q^2)$. The quantity σ_0 was separately determined for each W-bin and each model by minimizing the χ^2 of a fit vs. Q^2. In the GVDM, the form factor is given by

$$F_{GVDM}(Q^2) = F_T(Q^2) + F_L(Q^2), \tag{1}$$

with contributions from transverse (T) and longitudinal (L) photons:

$$F_T(Q^2) = \sum_{V=\rho,\omega,\phi} \frac{r_V}{\left(1 + Q^2/m_V^2\right)^2} + \frac{r_C}{1 + Q^2/m_0^2} \tag{2}$$

$$F_L(Q^2) = \sum_{V=\rho,\omega,\phi} \frac{r_V Q^2/4m_V^2}{\left(1 + Q^2/m_V^2\right)^2}, \tag{3}$$

where $r_\rho = 0.65, r_\omega = 0.08, r_\phi = 0.05$, $r_C = 0.22$, and $m_0 = 1.4$ GeV. Our VDM

form factor is identical to (1) with the r_C ("continuum") term omitted, and the coefficients r_V re-normalized so that their sum is 1. Note that the continuum term in the GVDM goes as $1/Q^2$ at large Q^2, and dominates the vector-meson pole terms above $\sim 1\,\mathrm{GeV}^2$; the longitudinal-photon contribution also has a $1/Q^2$ dependence at large Q^2. In the electroproduction process which the GVDM was designed to fit, the parton model associates $1/Q^2$ behavior with point-like photon-quark interactions. Thus, the GVDM already includes some part of the point-like cross section. Fits to hypotheses c) and d) were, in practice, obtained by subtracting the QPM expectation from the data, and then fitting according to a) and b), respectively. The QPM cross section was computed from that for $\gamma\gamma \to \mu^+\mu^-$, with quark masses substituted for the muon mass, and a factor of three included to account for colors:

$$\sigma^{QPM}_{\gamma\gamma\to q\bar{q}}(W,Q^2) \;=\; 3\sum_{q=u,d,s,c}\theta(W-2m_q)e_q^4\sigma_{\gamma\gamma\to\mu^+\mu^-}(W,Q^2,m_q). \qquad (4)$$

Quark masses were assigned as follows: $m_u = m_d = 325\,\mathrm{MeV}$, $m_s = 500\,\mathrm{MeV}$, and $m_c = 1.6\,\mathrm{GeV}$.

Table 1 shows the χ^2 values given by the fits; the fitted curves for the four hypotheses are included in Fig. 4. We also find that for the W bins between 3 and 10 GeV, the GVDM fits restricted to $0.2 < Q^2 < 1.6\,\mathrm{GeV}^2$ are all better per degree of freedom than the fits shown in Table 1, suggesting that using this form factor in the extrapolation to $Q^2 = 0$ was reasonable. None of the hypotheses works well for $2 < W < 3\,\mathrm{GeV}$, even in the Q^2 range below $1.6\,\mathrm{GeV}^2$. Over the range $3 < W < 10$ GeV, the data are best described by the VDM + QPM form factor, although the GVDM fits are quite similar. For the VDM + QPM fits in this

region, the σ_0 values - which correspond only to the VDM part of the cross section - all agree within the statistical errors, and average $416 \pm 25 \pm 46$ nb. Table 2 shows the fit σ_0 parameters, along with their statistical errors, for all four hypotheses. The GVDM + QPM ansatz which was found[10] to fit the PLUTO data fails to fit our data. We note that the Q^2-dependence of the Two-Gamma double-tagged data with $Q^2 < 1.6\,\mathrm{GeV}^2$ was found to be well-described by a GVDM form factor, again in agreement with the present measurement over the same Q^2 range.

It is clear from the fits shown in Table 1 that the VDM + QPM ansatz describes the data well over most of the W range. As mentioned above, an incoherent addition of these models may well double count. Various approaches have been suggested to circumvent this problem. Recent papers[15] suggest that the näive QPM calculation, which contains an implicit integral over the p_T of the outgoing quarks, be modified to cut off this distribution either at some minimum value of momentum transfer, or, equivalently, some p_T^{min}. We have used a p_T^{min} cut to modify[20] the QPM in fitting to the Q^2 dependence. In these fits we combined the unfolded result for $3 < W < 10\,\mathrm{GeV}$ into a single bin; the high-Q^2 data were also unfolded with this binning, and we include those results here to gain a larger lever arm in Q^2. The fits for different p_T^{min} values are summarized in Table 3; Fig. 5 shows the fitted curves for $p_T^{min} = 0$ and $1.0\,\mathrm{GeV}$, along with the GVDM curves. The fits are better when a p_T^{min} cut is made,[21] although even without a cut VDM + QPM is favored over GVDM. It is also apparent that increasing the value of p_T^{min} up to $1.0\,\mathrm{GeV}$ improves the GVDM + QPM fits. An additional feature (not shown in the table) of the p_T cutoff is that the fits to VDM + QPM for $2 < W < 3\,\mathrm{GeV}$ and $Q^2 < 6.8\,\mathrm{GeV}^2$ improve significantly, although they are still

poor: with $p_T^{min} = 0.5\,\mathrm{GeV}$, we find $\chi^2 = 23$ with 4 d.f., comparable to the χ^2 from the GVDM fit.

VI. CONCLUSION

In summary, we have measured the total cross section for $\gamma\gamma \to$ hadrons as a function of both W and Q^2. We find that over most of the available W range, $3 \lesssim W < 10$ GeV, the Q^2 dependence of the data is well represented by a sum of vector-meson terms and a point-like contribution, using the QPM with constituent quark masses. This model also works at high Q^2, where it is possible to distinguish between this and a simple GVDM form factor. Using an improved parton model with a cut on the minimum p_T of the outgoing quarks (to avoid double-counting with the VDM contribution) gives an even better fit to the Q^2 dependence. The cross section extrapolated to $Q^2 = 0$ shows a rather gentle fall-off with W.

Acknowledgments

We acknowledge the efforts of the PEP staff and engineers, and thank them for productive running. We also thank John H. Field for useful discussions. This work was supported in part by the United States Department of Energy (under contracts DOE–W–7405–Eng–82, DE–AT03–89ER40492, DE–AS03–76ER70285, DE–AT03–88ER40384, DE–AT03–87ER40327, DE–AT03–79ER70023, DE–AC03–76SF00098, DE–AC02–85ER40194, and DE–AC03–76SF00515), the National Science Foundation (under grants PHY89–07526 and PHY88–19536), the Joint Japan-United States Collaboration in High Energy Physics, and the Foundation for Fundamental Research on Matter in The Netherlands.

Appendix: $A + B/W$ Fits, and Sensitivity to Unfolding

In Figure 3, we presented our results for the $Q^2 = 0$ cross section for $\gamma\gamma \to$ hadrons as a function of the $\gamma\gamma$ center of mass energy W. While we do not wish to place undue emphasis on these extrapolated results, it has become traditional to describe this and other low-energy cross sections by fits of the form $\sigma = A + B/W$. A reader attempting to construct such a fit to our results would be misled, because cross sections – like ours – which are extracted with the Blobel unfolding procedure[9] have substantial correlations (of both signs) between W bins. In this Appendix, we discuss $A + B/W$ fits with correlations taken into account, and we also comment on the sensitivity of our results to details of the unfolding procedure.

Fits have been carried out by minimizing the quantity

$$\chi^2 = \sum_{i,j} (\sigma_i^{fit} - \sigma_i) E_{ij}^{-1} (\sigma_j^{fit} - \sigma_j)$$

as a function of the fit parameters. Here i and j run over the unfolded W bins of interest, and E_{ij} is the error matrix which, along with the "measured" cross sections σ_i, is provided by the unfolding program. Systematic uncertainties are not included in the fits, because they have a strong positive correlation between all bins. If we fit the entire range $2 < W < 10\,\mathrm{GeV}$ to $A + B/W$, we obtain $A = 388 \pm 19\,\mathrm{nb}$ and $B = 153 \pm 58\,\mathrm{nb\,GeV}$. However, A and B are close to 100% negatively correlated, so that the one standard deviation band of fit cross sections is relatively narrow. This band is shown in Fig. A1, along with our σ_i results as in Fig. 3. The fit is in fact not very good; its χ^2 value and other parameters are summarized in Table A1, along with those for additional fits to be described.

Because the GVDM extrapolating function does not describe our data well in the lowest W bin (see Section V.C and Table 1), we have also fit the same unfolded data to $A + B/W$ for the more restricted range $3 < W < 10\,\mathrm{GeV}$. The results of this fit are also shown in Figure A1 and Table A1.

We next consider the sensitivity of our results to details of unfolding. The unfolding program is provided with event-by-event measured values of W_{vis}, and with the W and W_{vis} values for the Monte Carlo events; the Monte Carlo events allow the program to obtain the correlation between the two variables. The primary control input to the program is a parameter N, which is interpreted as the number of roughly independent bins of W over the range of interest, using bin sizes consistent with experimental resolution. The program fits the true W distribution to a sum of orthogonal oscillating functions (linear transformations of cubic B-splines), where the number of terms effectively contributing is close to N. Results (for N terms) may then be displayed in "optimized" bins, chosen by the program to minimize correlations introduced by term $N + 1$. We have instead used results integrated over specific fixed W-bins, in order to facilitate comparisons of different Q^2 regions, values of N, etc.

All of the results presented in Section V, and hence the W fits described above, were obtained with the value $N = 4$. However, within a small range of values, there is no *a priori* correct choice. Hence we need to consider the variation of this parameter in our systematic uncertainty. Table A1 gives the results of unfolding with $N = 5$ as opposed to our usual choice of $N = 4$. The changes in A and B for $N = 5$ vs. $N = 4$ reflect changes in the unfolded $Q^2 = 0$ cross section values themselves, a variation we have allowed for in our systematic uncertainty

estimates. Note that this systematic error does *not* occur for our primary results, the cross sections in Q^2 bins (Section V.C). There, the 4- and 5-point results agree within our statistical errors: only four of the twenty data points shown in Fig. 4 change by more than one error bar.

We have also considered fits of the form $\sigma = \sigma_{QPM}(W) + A + B/W$, where $\sigma_{QPM}(W)$ is the $Q^2 = 0$ limit of Eq. (2). The results for σ^{fit} for $2 < W < 10\,\mathrm{GeV}$ are close to the corresponding $A + B/W$ results. This is because over this W range the QPM cross section falls only about twice as much as a $1/W$ form (in contrast to the $1/W^2$ dependence frequently ascribed to this cross section). Hence A values determined by the fits come out about the same, while B values are reduced by about $250\,\mathrm{nb\,GeV}$. (The negative B values thus obtained in some cases may be further evidence of the double-counting mentioned in Section II.)

Despite the poor quality of the $A + B/W$ fits, they may be compared to previously-published values. Especially when systematic uncertainties are allowed for, all the variations given in Table A1 are compatible with the Two-Gamma double-tag results ($A = 360 \pm 60\,\mathrm{nb}$ and $B = 10 \pm 290\,\mathrm{nb\,GeV}$), but not with the PLUTO single-tagged results ($A = 107 \pm 40\,\mathrm{nb}$ and $B = 933 \pm 112\,\mathrm{nb\,GeV}$). However, comparing A and B values tends to exaggerate the differences between experiments. Actual differences are more fairly represented by Figure 3 itself.

REFERENCES

1. Ch. Berger and W. Wagner, *Phys. Rep.* **146**, 1 (1987).

2. H. Kolanoski, *Two Photon Physics at e^+e^- Storage Rings*, Springer-Verlag (1984).

3. *Proceedings of the VI^{th} International Workshop on Photon-Photon Collisions*, R.L. Lander, ed., World Scientific (1985).

4. *Proceedings of the VII^{th} International Workshop on Photon-Photon Collisions*, P. Kessler and A. Courau, eds., World Scientific (1986).

5. John H. Field in *Proceedings of the $VIII^{th}$ International Workshop on Photon-Photon Collisions*, U. Karshon, ed., World Scientific (1988).

6. H. Aihara *et al.*, *Z. Phys.* **C34**, 1 (1987).

7. H. Aihara *et al.*, "*Measurement of the Photon Structure Function at* $10 < Q^2 < 60\,\mathrm{GeV}^2$," University of Massachusetts Report UMHEP-325 (1989), to be submitted for publication.

8. V.M. Budnev, I.F. Ginzburg, G.V. Meledin, and V.G. Serbo, *Phys. Rep.* **15C**, 181 (1975).

9. V. Blobel, DESY Report 84-118 (1984).

10. Ch. Berger *et al.*, *Z. Phys.* **C26**, 353 (1984).

11. Ch. Berger *et al.*, *Phys. Lett.* **149B**, 421 (1984).

12. D.L. Bintinger *et al.*, *Phys. Rev. Lett.* **54**, 763 (1985).

13. S.E. Baru *et al.*, *contributed paper to the $XXIII^{rd}$ International Conference in High Energy Physics*, Berkeley, 1986, and Novosibirsk Preprint 86-106 (1986).

14. M. Feindt, in *Proceedings of the VII^{th} International Workshop on Photon-Photon Collisions, ibid.*, p. 388.

15. J.H. Field, F. Kapusta, and L. Poggioli, *Phys. Lett.* **181B**, 362 (1986), and *Z. Phys.* **C36**, 121 (1987).

16. H. Aihara *et al.*, *"Charged Hadron Production in e^+e^- Annihilation at $\sqrt{s} = 29\,GeV$"*, LBL Report LBL-23737 (1988).

17. T. Sjostrand, *Com. Phys. Comm.* **27**, 243 (1982); **28**, 229 (1983); B. Andersson *et al.*, *Phys. Rep* **97**, 31 (1983). Version 5.3 of the software package was used.

18. J.J. Sakurai and D. Schildknecht, *Phys. Lett.* **40B**, 121 (1972).

19. It should be noted that none of these experiments is sensitive to final states of just two hadrons. While both the present analysis and that of PLUTO make small acceptance corrections (implicit in the multiplicity models) for this omission, the actual cross section for such states near $W = 2\,\mathrm{GeV}$ may be larger than is allowed for.

20. C. Hill and G. Ross, *Nuc. Phys.* **B148**, 373 (1979). We use eq. 1.6a to deduce $d\sigma/dp_T$ for the case $P^2 \to 0$, where $-P^2$ is the mass squared of the target photon.

21. As the value of p_T^{min} is increased from 0 to 0.5 GeV, χ^2 for the QPM + VDM fit falls approximately linearly.

Fit	$2 < W < 3$	$3 < W < 4$	$4 < W < 6$	$6 < W < 10$
VDM	62	65	41	2.2
GVDM	19	7.7	8.6	12.4
VDM+QPM	49	5.5	6.7	8.8
GVDM+QPM	99	26	28	36

Table 1. χ^2 values for fits with 4 d.f., to the data vs. Q^2 ($0.2 < Q^2 < 6.8\,\mathrm{GeV}^2$). The four models are described in the text.

Fit	$2 < W < 3$	$3 < W < 4$	$4 < W < 6$	$6 < W < 10$
VDM	629 ± 31	652 ± 39	578 ± 41	515 ± 53
GVDM	452 ± 22	476 ± 28	413 ± 29	350 ± 36
VDM+QPM	320 ± 31	424 ± 39	407 ± 41	417 ± 53
GVDM+QPM	213 ± 22	295 ± 28	279 ± 29	272 ± 36

Table 2. σ_0 values (in nb) determined by fits whose χ^2's are shown in Table 1. Errors are statistical only.

Fit	$p_T^{min} = 0$	$p_T^{min} = 0.5$	$p_T^{min} = 1.0$	$p_T^{min} = 1.5$
VDM	55	-	-	-
GVDM	22	-	-	-
VDM+QPM	14.1	7.9	6.7	7.9
GVDM+QPM	80	61	48	48

Table 3. χ^2 values for fits with 6 d.f., using QPM modified to cut off at various values of p_T^{min} (GeV), for $3 < W < 10\,\mathrm{GeV}$, and $0.2 < Q^2 < 60\,\mathrm{GeV}^2$.

W (GeV)	N	χ^2 (DF)	A (nb)	B (nb GeV)	C_{AB}
2–10	4	14.9 (3)	388 ± 19	153 ± 58	-0.94
3–10	4	12.0 (2)	349 ± 29	356 ± 132	-0.96
2–10	5	11.7 (3)	335 ± 26	387 ± 94	-0.96
3–10	5	11.1 (2)	356 ± 38	275 ± 179	-0.97

Table A1. Results of fits of the extrapolated $Q^2 = 0$ cross section to the form $A + B/W$. N is the unfolding parameter described in the Appendix, and C_{AB} is the correlation between A and B.

Figure Captions

1. The two-photon reaction in e^+e^- collisions. Shown are lab frame four-momenta and angles.

2. (a) The unfolded cross section at an average Q^2 of (a) $0.44\,\mathrm{GeV}^2$, and (b) $4.5\,\mathrm{GeV}^2$, compared to PLUTO data from Ref. 10. All error bars are statistical only.

3. The cross section extrapolated to $Q^2 = 0$, compared to similar extrapolations by the Two-Gamma[12] and PLUTO[11] collaborations. The plotted error bars are statistical only. (The Two-Gamma measurement remains approximately flat to its maximum W of 20 GeV.)

4. Q^2 dependence of the cross section in four bins of W. Error bars are statistical only. The curves are fits to the four hypotheses described in the text.

5. Q^2 dependence of the cross section for $3 < W < 10$ GeV, including points at high Q^2. Error bars are statistical only.

A1. Extrapolated cross section, as in Fig. 3, along with $\pm 1\sigma$ bands from $A + B/W$ fits. The solid curves enclose the band for the fit over $2 < W < 10\,\mathrm{GeV}$, while the dot-dash curves enclose the band for the fit over $3 < W < 10\,\mathrm{GeV}$.

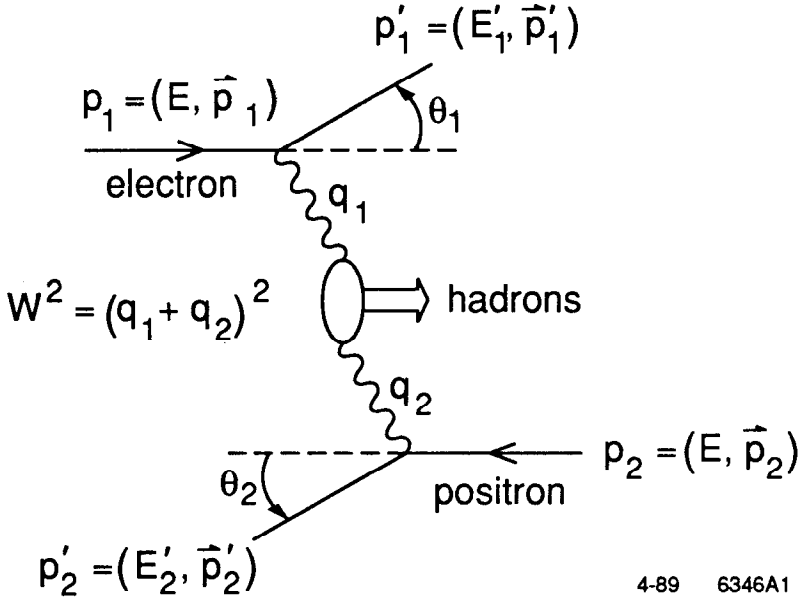
$p_1' = (E_1', \vec{p}_1')$
$p_1 = (E, \vec{p}_1)$
θ_1
electron
q_1
$W^2 = (q_1 + q_2)^2$
hadrons
q_2
$p_2 = (E, \vec{p}_2)$
θ_2
positron
$p_2' = (E_2', \vec{p}_2')$
4-89 6346A1

Fig. 1

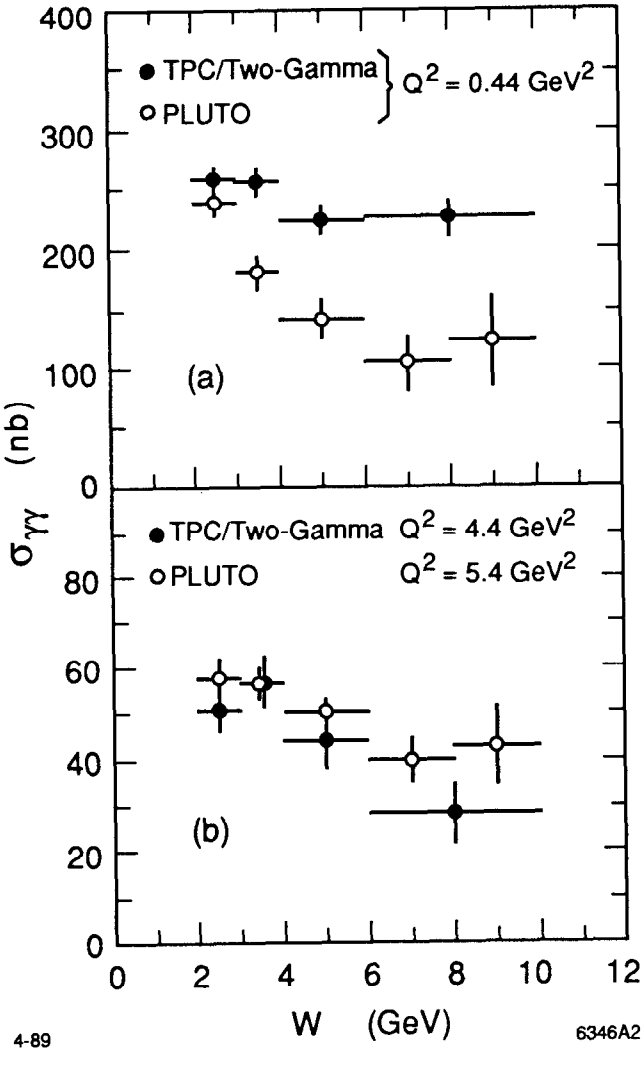
400
300
200
100
0
● TPC/Two-Gamma
○ PLUTO
Q^2 = 0.44 GeV^2
(a)
$\sigma_{\gamma\gamma}$ (nb)
80
60
40
20
0
● TPC/Two-Gamma Q^2 = 4.4 GeV^2
○ PLUTO Q^2 = 5.4 GeV^2
(b)
0 2 4 6 8 10 12
W (GeV)
4-89
6346A2

Fig. 2

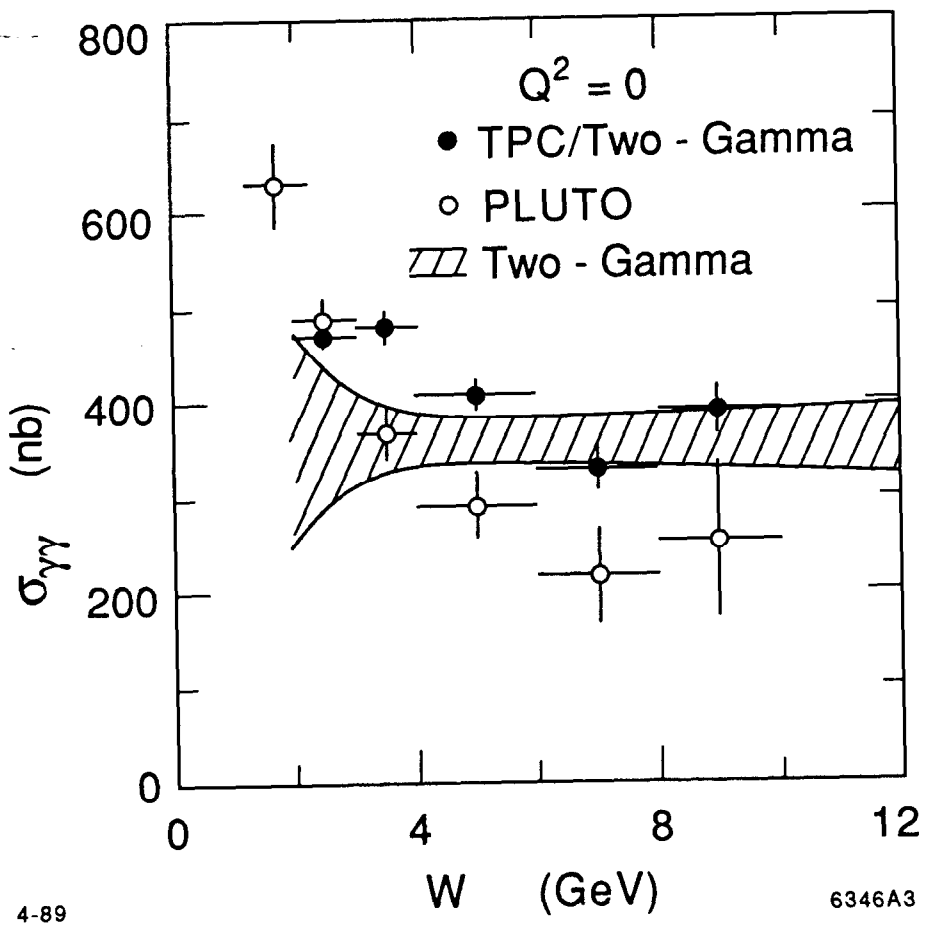
800
600
400
200
0
$Q^2 = 0$
TPC/Two - Gamma
PLUTO
Two - Gamma
$\sigma_{\gamma\gamma}$ (nb)
0
4
8
12
W (GeV)
4-89
6346A3

Fig. 3

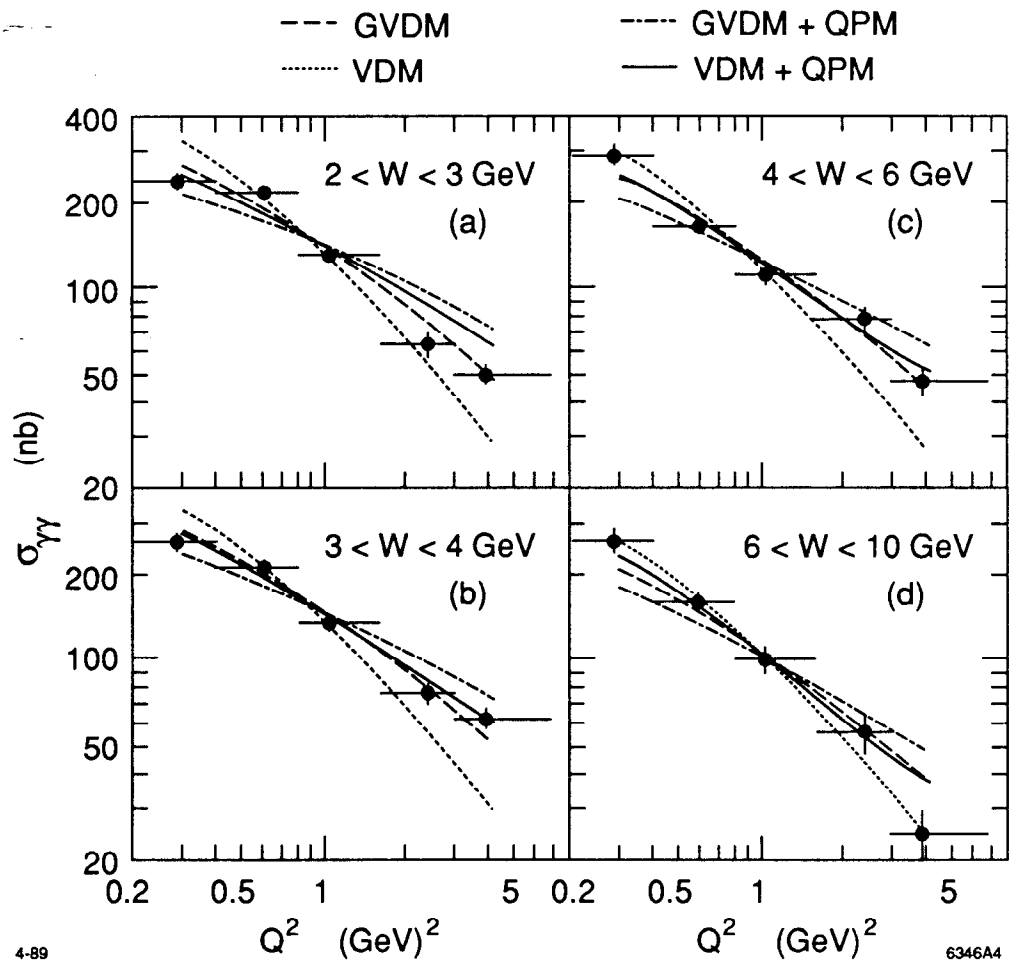
GVDM
VDM
GVDM + QPM
VDM + QPM
2 < W < 3 GeV
(a)
4 < W < 6 GeV
(c)
3 < W < 4 GeV
(b)
6 < W < 10 GeV
(d)
$\sigma_{\gamma\gamma}$ (nb)
400
200
100
50
20
0.2
0.5
1
5
Q^2 $(GeV)^2$
4-89
6346A4

Fig. 4

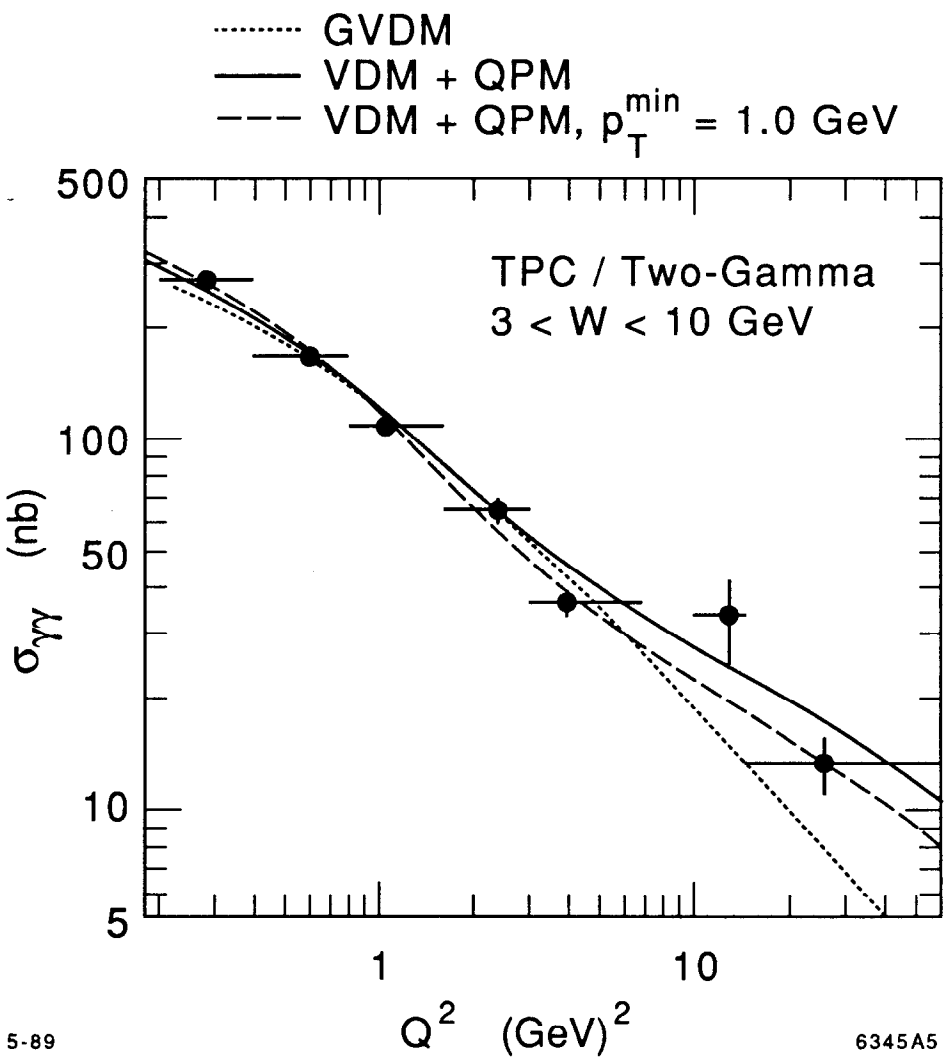
GVDM
VDM + QPM
VDM + QPM, p_T^{min} = 1.0 GeV
TPC / Two-Gamma
3 < W < 10 GeV
500
100
50
10
5
$\sigma_{\gamma\gamma}$ (nb)
1
10
Q^2 $(GeV)^2$
5-89
6345A5

Fig. 5

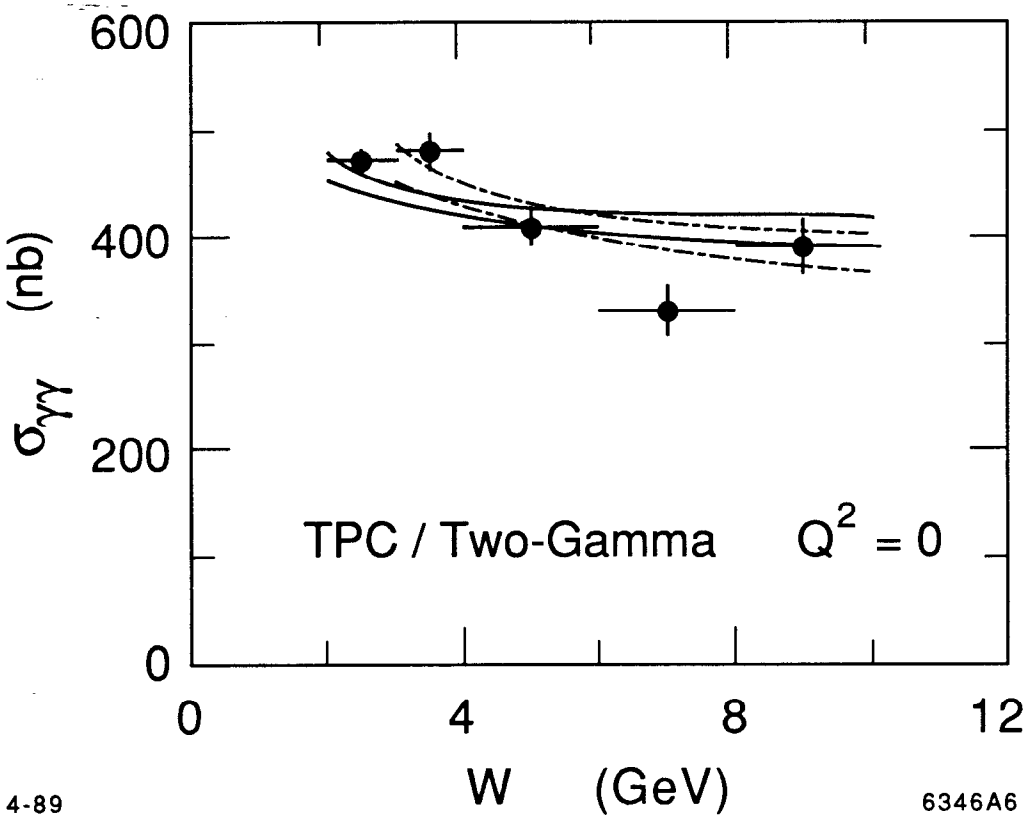
600
400
200
0
$\sigma_{\gamma\gamma}$ (nb)
TPC / Two-Gamma $Q^2 = 0$
0
4
8
12
W (GeV)
4-89
6346A6

Fig. A1